A Moderately Strong Photoacid Dissociates in Alcohols with High Transient Concentration of the Proton-Transfer Contact Pair

Alfonso Brenlla,[†,‡] Manoel Veiga Gutiérrez,[†,¶] M. Carmen Ríos Rodríguez,[†] Flor Rodríguez-Prieto,[†] Manuel Mosquera,[*,†] and J. Luis Pérez Lustres[*,†]

Center for Research in Biological Chemistry and Molecular Materials (CIQUS) and Department of Physical Chemistry, University of Santiago de Compostela, E-15782 Santiago de Compostela (Spain)

E-mail: manuel.mosquera@usc.es; luis.lustres@usc.es

Phone: +34 8818 15722. Fax: +34 8818 15704

[*]To whom correspondence should be addressed

[†]CIQUS

[‡]now at Department of Chemistry, Wayne State University, 5101 Cass Avenue, Detroit, MI 48202 (USA)

[¶]now at PicoQuant GmbH, Kekuléstr. 7, 12489 Berlin (Germany)

Abstract

Proton transfer from strong photoacids to hydroxylic solvents is much under debate. Experimentally, the main issue stems from relaxation and diffusion processes that are concomitant with ultrafast proton transfer, and blur population dynamics. To overcome this, we propose a fast photodissociation reaction that, however, proceeds slower than solvent relaxation. Fluorescence spectroscopy of the cationic photoacid 2-(1'-hydroxy-2'-naphtyl)benzimidazolium reveals a two-stage mechanism: (a) reversible elementary proton transfer inside the solvent shell, and (b) irreversible contact-pair splitting. The time-evolution of the fluorescence signal is complex, yet this is explained quantitatively by simultaneous, spectrally overlapping emission of the acid, the conjugate base and the contact proton-transfer pair. The latter attains high transient concentration in linear alcohols. Microscopic rate constants of dissociation are determined.

Graphical TOC Entry

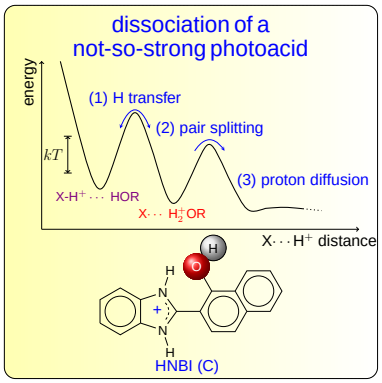

KEYWORDS: Proton Transfer, Fluorescence Spectroscopy, Time-Resolved Spectroscopy, Acids and Bases, Solution Chemistry, Kinetics and Photochemistry

Proton transfer (PT) is one of the most relevant processes in chemistry [1–3] and is ubiquitous in biology. [4] The reaction implies exchange of a proton between two centers and is often accompanied by strong charge redistribution. [5,6] Modern reaction models have firmly established the quantum behavior of the fast-moving proton and the role of the "slow" solvent as actual promoter of the elementary PT step. [7–13] Thus, solvent reorganization tunes the proton transfer potential and thereby enables proton displacement along a preexisting hydrogen bond. Unfortunately, the insightful view contributed by theoretical chemistry is hard to corroborate experimentally.

Formally, intermolecular PT reactions occur via the Eigen–Weller three-stage mechanism: [1,3,14] diffusional approach of reactants (AH and B) to form the encounter complex AH$\cdots$B, proton exchange in the complex to form the contact ion pair ($A^- \cdots {}^+HB$) and last, product separation by diffusional motion. Consequently, the fastest PT reactions are diffusion controlled, the encounter complex reaches negligible transient concentrations in the course of the reaction and the characteristic rate constant contains little information about the elementary PT step. This can be avoided with the aid of photoacids. [15] These compounds become much more acidic in the first-excited singlet state. In this way, the (AH$\cdots$B) encounter complex may be populated directly by a short laser pulse and all subsequent reaction stages may be probed by time-resolved optical spectroscopy in proton-accepting solvents.

Time-resolved optical spectroscopy of strong photoacids reveals complex photodissociation kinetics, which has been interpreted from essentially two different perspectives. First, it has been recognized that photoacid behavior entails strong electronic reorganization. [5,6] The latter triggers solvent relaxation, which drives the elementary PT step in the adiabatic limit. [13,16] Solvent relaxation induces a dynamic spectral shift concomitant with the PT reaction, so that kinetic traces measured at single wavelengths suggest "accelerated" dynamics arising from both spectral and population evolution in time. The correction for this effect exposes the underlying exponential kinetics, which is consistent with the classical Eigen–Weller mechanism. Sizeable transient concentration of the $A^- \cdots {}^+HB$ contact ion pair was deduced. [17,18] This interpretation is supported by molecular dynamics simulations, which predict the build-up of the contact pair during dissociation of simple

moderate acids.[19,20] In some other cases, geminate proton-conjugate base recombination[3,21,22] was invoked to explain non-exponential dynamics. Both kinetic models were applied independently to the photodissociation of the strong photoacid N-methyl-6-hydroxyquinolinium,[16,23] for which a $\approx$ 3000 cm^{-1} solvation shift of the conjugate base was experimentally demonstrated.[18,24] The remaining of this letter is devoted to the study of proton transfer to solvent (PTTS) in a moderately strong photoacid. The elementary PT step is significantly slower than solvent dynamics, so that possible interferences from intramolecular charge redistribution or solvent dynamics can be readily discriminated.[13] Proton ejection and splitting of the proton-transfer pair are assessed directly.

In this work, we study the proton transfer from the cationic photoacid 2-(1'-hydroxy-2'-naphtyl) benzimidazolium (HNBI) to alcohols by steady-state and single-wavelength ps single-photon counting fluorescence spectroscopy, and spectral reconstruction. The general photochemical behavior of HNBI was described previously.[25] Briefly, HNBI (cation **C**, see Scheme 1) dissociates in the first-excited singlet state to afford the neutral tautomer **T*** in water and alcohols. Both species contribute to the stationary fluorescence spectrum measured in acidified alcohols. See Reference 25 for further details.

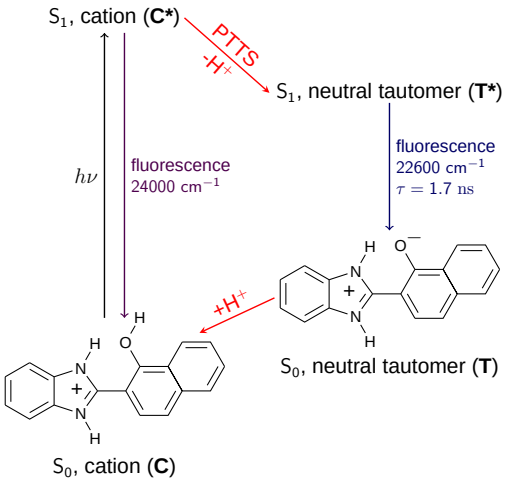

Scheme 1: Excitation and deactivation pathways of HNBI in acidified alcohols.

Figure 1 shows the fluorescence excitation and emission spectra of HNBI in acidified alcohols.

The excitation spectrum does not depend on solvent and corresponds to that of the cationic form.[25] In turn, fluorescence emission is dual. The shoulder observed at about 25000 cm^{-1} corresponds to the emission of **C***, which is the only species emitting in nonbasic solvents like acetonitrile. The main fluorescence band, which peaks at $\approx$ 22500 cm^{-1}, was assigned to the excited neutral tautomer **T***, implying that PTTS occurs in the excited electronic state S_1.[25]

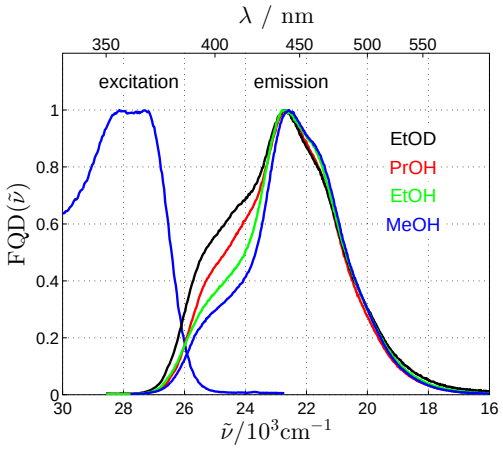

Figure 1: Normalized fluorescence spectrum of HNBI (shown as quantum distribution over wavenumbers, FQD($\tilde{\nu}$)) measured in methanol (MeOH), ethanol (EtOH), deuterated ethanol (EtOD) and 1-propanol (PrOH) in acidic conditions ($[HClO_4]$ = 0.01 M).

We measured the fluorescence decay of HNBI in acidic methanol at 29 independent emission wavelengths across the full emission spectrum. The range from 380 to 520 nm was scanned. Fluorescence decays in a complex manner upon excitation of **C**. Decay traces were analyzed globally with bi- and tri-exponential functions. The best global fit is triexponential with decay times τ_{1-3} of 0.43, 0.71 and 1.6 ns (Figure 2 and Figure SI 1). We remark however that τ_1 and τ_2 are very similar and they can only be discriminated by global analysis. This is further confirmed by the trend observed in other alcohols, where the two decay times diverge. Bi- and triexponential global fits are compared in Supporting Information (Figures SI 1-5). Figures SI 6-10 provide a summary of the global triexponential fit in methanol. Here, we underline the following observations: first, all three time-zero amplitudes A_{1-3} are positive in the blue spectral range ($\lambda_{em} < 430$ nm), but $A_{1,2}$

become increasingly negative in the red (Figure SI 6). Second, independent measurements in neutral methanol show that $\tau_3 = 1.6$ ns is the decay time of **T***.[25] Finally, $\tau_{1,2}$ are much shorter than the fluorescence decay time of **C*** (2.4 ns in acidic acetonitrile[25] and trifluoroethanol, where no PTTS reaction occurs) and significantly longer than the characteristic solvation time of methanol, 3 ps.[18,24] We note that the instrument response function (IRF) of the single-photon counting experiment here described is 90 ps and the highest time resolution achievable is estimated to be 10 ps. Therefore, most of the solvation response goes unnoticed. Only the slowest diffusional stage of solvation could be resolved. But the latter has a characteristic time constant of $\approx$ 40 ps in methanol, [18] and is still much faster than $\tau_{1,2}$. Therefore, one can safely conclude that $\tau_{1,2}$ are associated to the PTTS reaction in methanol. To summarize, HNBI proton transfer to methanol shows plain triexponential behavior with no interference of spectral dynamics by solvent relaxation. Similar results were obtained for ethanol, deuterated ethanol and 1-propanol.

The above described behavior is consistent with the classical Eigen–Weller[1,14] model (Scheme 2) under the assumption of irreversible splitting of the proton-transfer contact pair **T***$\cdots H^+$ (**P*** for brevity). Thus, we assume that the excited HNBI cation dissociates and forms the proton-transfer contact pair (**P***). The process is reversible and the rate constants k_1 and k_{-1} are defined for the forward- and back-reactions. **P*** may further split with a rate constant k_2 to form the conjugate base **T*** and the free proton, or decay to the ground-electronic state. The decay constant is assumed to be the same for **P*** and free **T***, namely k_T. We find no indication for recombination in the second stage, i.e. $k_{-2}\,[H^+] << k_2, k_T$.

Analytical forms of the time-dependent concentrations are summarized in eqs (1). The assumption was made that the initial concentration of **C*** is c_0, whereas those of **P*** and **T*** are zero. The

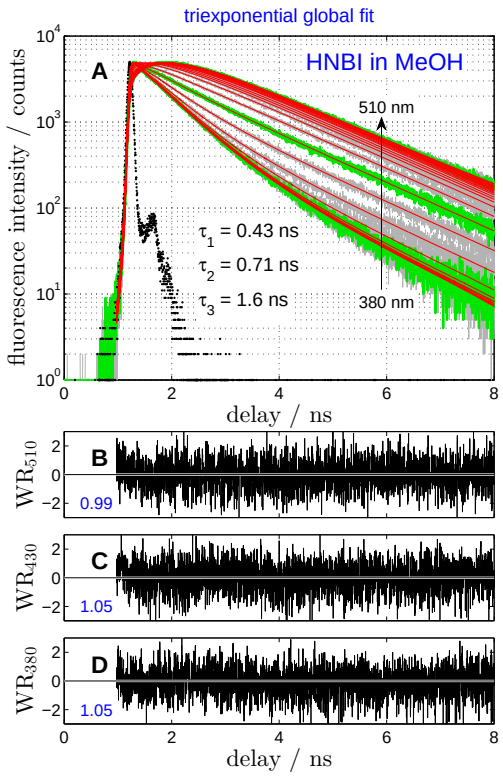

Figure 2: Fluorescence decay curves of HNBI measured from 380 to 510 nm every 5 nm in methanol (gray lines, Panel A). Results from a global triexponential fit (red lines) are shown together with the excitation pulse (black dots). Green curves highlight three representative wavelengths for which weighted residuals (WR_λ) are shown in panels B-D, where normalized χ^2_N values are indicated in blue for each emission wavelength λ.

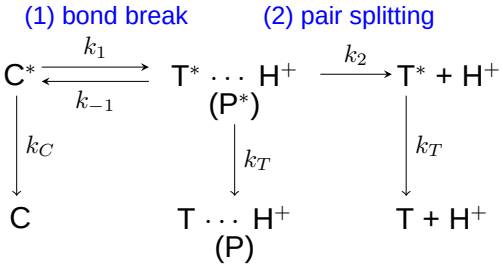

Scheme 2: Proposed mechanism for the photodissociation of the HNBI cation **C*** in alcohols.

$$[\mathrm{C}^*(t)] = \frac{c_0}{\beta_1 - \beta_2}\left[(X-\beta_2)e^{-\beta_1 t} - (X-\beta_1)e^{-\beta_2 t}\right] \tag{1a}$$

$$[\mathrm{P}^*(t)] = \frac{c_0(X-\beta_1)(X-\beta_2)}{k_{-1}(\beta_1-\beta_2)}\left[e^{-\beta_1 t} - e^{-\beta_2 t}\right] \tag{1b}$$

$$[\mathrm{T}^*(t)] = \frac{c_0(X-\beta_1)(X-\beta_2)}{(\beta_1-\beta_2)}\frac{k_2}{k_{-1}}\left[\frac{e^{-\beta_1 t}}{\beta_3-\beta_1} - \frac{e^{-\beta_2 t}}{\beta_3-\beta_2} - \left(\frac{1}{\beta_3-\beta_1} - \frac{1}{\beta_3-\beta_2}\right)e^{-\beta_3 t}\right] \tag{1c}$$

definitions in eqs (2) were used. It is deduced that **C*** evolves biexponentially, with lifetimes β_1^{-1} and β_2^{-1} (eq (1a)). The preexponential factors depend on all rate constants in an intricate manner. Similarly, the encounter pair **P*** evolves biexponentially in time, shows the same lifetimes as **C***, but different preexponential factors (eq (1b)). Finally, the time-dependent concentration of **T*** is triexponential with lifetimes β_1^{-1}, β_2^{-1} and k_T^{-1} (eq (1c)).

$$X = k_1 + k_C \tag{2a}$$

$$Y = k_2 + k_T + k_{-1} \tag{2b}$$

$$Z = \sqrt{(X-Y)^2 + 4k_1k_{-1}} \tag{2c}$$

$$\beta_1 = \frac{1}{2}(X + Y + Z) \tag{2d}$$

$$\beta_2 = \frac{1}{2}(X + Y - Z) \tag{2e}$$

$$\beta_3 = k_T \tag{2f}$$

According to Scheme 2, the time-resolved fluorescence intensity $F(\nu, t)$ is a linear superposition of the time-dependent concentrations of **C***, **P*** and **T***. The contribution of each species i depends on the relative weight of the corresponding species-associated spectrum (SAS) $F_i(\nu)$ at the emission frequency ν, i.e. $F(\nu,t) = F_C(\nu)[\mathrm{C}^*(t)] + F_T(\nu)([\mathrm{P}^*(t)] + [\mathrm{T}^*(t)])$. The emission spectra of **P*** and **T*** are expected to be indistinguishable at our spectral resolution of ≈ 200 cm^{-1}. Nevertheless, **P*** and **T*** may be readily discriminated by their distinct time evolution.[18] Therefore, a global analysis of the fluorescence decay reports first, the microscopic rate constants of the PTTS reaction and second, the fluorescence spectra associated to the participating species.[26] In the fitting procedure, and in order to reduce parameter correlations, k_C was assumed to be (2.35 ns)$^{-1}$. This is the fluorescence decay rate constant measured in acidic acetonitrile and trifluoroethanol, where no photodissociation takes place.[25] Remarkably, the target analysis with amplitudes and lifetimes restricted to the analytical forms in eqs (1) is as good as the free triexponential global fit shown in Figure 2 (see Table SI 1 and Figures SI 5–9 in the Supporting Information). This is a quite

stringent condition because the rate constants of the free fit might not fulfill the amplitude ratios derived from the Eigen–Weller model. But quite the opposite, the target analysis converges to the same rate constants as the free global fit, is able to narrow down the uncertainties of the fitted parameters and resolve the combination of rate constants X. The so-deduced time-dependent contributions of all emitting species are represented in Figure 3. Noteworthy, the analysis shows that the concentration of the contact pair is highest at 2 ns and vanishes on the 10 ns timescale.

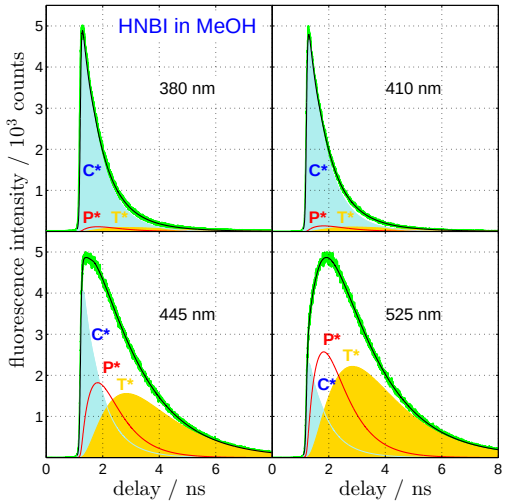

Figure 3: Calculated time-dependent contributions of the different species to the fluorescence decay of HNBI in MeOH at the indicated emission wavelengths. The cation (**C***) is shown in blue, the proton-transfer contact pair (**P***) in red and the neutral tautomer (**T***) in orange. Experimental fluorescence traces are shown in green and the fitted curves resulting from the target analysis are shown in black.

The optimized rate constants are examined now (Table 1). First, the fitted values of k_T range from 0.55 ns^{-1} in 1-propanol to 0.65 ns^{-1} in methanol. They agree with those extracted from the monoexponential fluorescence decays measured in different neutral solvents of similar refractive indexes: 0.59 ns^{-1} in ethanol and 0.65 ns^{-1} in acetonitrile. Second, k_2 is close to 1 ns^{-1}, which is slightly below the diffusion-control limit.[18] This indicates that, in this case, the splitting of the proton-transfer pair has an activation energy of about $2 \times kT$. Next, the kinetic isotope effect (KIE) is obtained from measurements in ethanol and ethanol–d_1 at the same $HClO_4$ concentration.

The proton exchange rate is fast, so that virtually all HNBI hydroxy groups are deuterated in ethanol−d_1. The microscopic rate constants k_1, k_{-1} and k_2 change only slightly upon deuteration. This leads to a KIE $= \vec{k}_H/\vec{k}_D$ of ≈ 2.3 when the isotope effect is quantified, as usual, via the macroscopic rate constant for the forward reaction $\vec{k} = \dfrac{k_1 k_2}{k_{-1} + k_2}$.[1] Whereas the scarce information available hinders a more profound analysis, it can be advanced that the small KIE arises from a very loose O−H vibration in the excited state, from reaction asymmetry or from the involvement of the solvent coordinate.[27]

We analyze now the pair-splitting stage and set a higher bound for the HNBI recombination rate constant k_{-2} in alcohols. The comparison of the experimental value of k_2 with the diffusion rate constant[18] indicates that the barrier for the splitting of the proton-transfer pair is $\approx 2 \times kT$. Next, one observes that the proton transfer kinetics of HNBI remains unchanged after a ten-fold increase in the proton concentration from 0.01 M to 0.1 M (Table 1). The latter implies that proton recombination does not take place to a significant extent in the experiments here described, i.e. $k_{-2} \times$ 0.1 M is much smaller than k_2, k_T. Therefore, k_{-2} is ≤ 1 ns^{-1} M^{-1} and lays at least ten times below the diffusion-control limit. Altogether, one concludes that the forward and back reactions of the pair-splitting stage are activated by a few kT. This means that the hydrogen-bond interaction between the leaving proton and the conjugate base is still significant in the pair and the proton has to surmount a second energy barrier before it can diffuse freely. Thus, proton diffusion remains dark in our experiment because the process does not affect the concentration of the fluorescent conjugate base.

Table 1: Rate constants (in ns^{-1}) obtained from the target analysis of fluorescence decay curves.

Solvent	[$HClO_4$]/M	k_1	k_{-1}	k_2	k_C[a]	k_T
methanol	0.01	1.3	0.2	1.2	0.42	0.65
ethanol	0.01	1.1	0.4	1.3	0.42	0.59
ethanol-d	0.01	0.5	0.3	0.8	0.42	0.56
ethanol	0.10	1.4	0.5	1.4	0.42	0.57
1-propanol	0.01	0.8	1.0	1.2	0.42	0.55

[a] Kept constant in the fit.

The amplitudes associated to the kinetic traces of each species shown in Figure 3 can be used to calculate by spectral reconstruction the species-associated-spectra (SAS).[26] For this purpose the fluorescence decay curves $F(\nu, t)$ are integrated for all emission frequencies and compared to the stationary emission spectrum in the same solvent FQD(ν). The correction factors $\chi(\nu)$ are calculated as $\frac{\text{FQD}(\nu)}{\int F(\nu,t)dt}$. Therefore, the SAS are obtained as the product of the spectral amplitude associated to a given species (Figure SI 12) and the correction factor $\chi(\nu)$. Results are shown in Figure 4 and compared to the emission spectra of **C*** and **T*** measured independently. The agreement between both sets of spectra is very good, supporting thereby the proposed mechanism (Scheme 2).

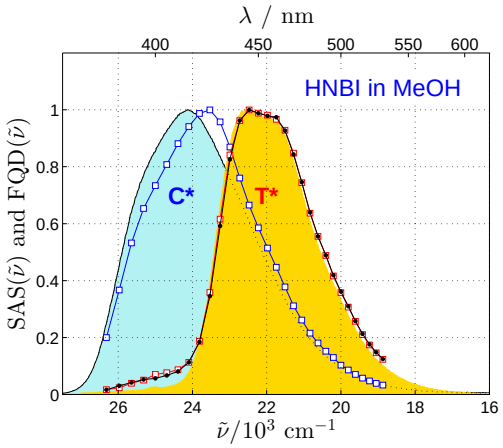

Figure 4: Species-associated spectra (SAS) of the cation (**C***, blue squares) and the tautomer (**T***, red squares) as deduced from spectral reconstruction of time-zero amplitudes in methanol. Fluorescence spectra (shown as quantum distributions (FQD)) were obtained by steady-state fluorescence spectroscopy and are shown as filled curves: the HNBI cation (light blue) was measured in acidic acetonitrile while the tautomer (light orange) was obtained in neutral methanol. The reconstructed spectrum of the reaction intermediate (**P***, black dots) is indistinguishable from that of the tautomer at our spectral resolution. The reconstructed time-dependent fluorescence emission spectra are shown in the Supporting Information, Figure SI 10.

We conclude, photodissociation of HNBI in acidified alcohols fulfills the Eigen–Weller mechanism. The reaction can be probed precisely by picosecond fluorescence spectroscopy. No interference of spectral evolution by intramolecular charge redistribution or solvent dynamics was

detected. No indication of proton-to-base recombination was observed. Remarkably, the proton-transfer contact pair achieves high concentration during the earliest 1-2 ns of the reaction. Similar findings were reported for the stronger photoacid N-methyl-6-hydroxyquinolinium,[18] but for a different reason. Ultrafast, barrierless dissociation of the quinolinium photoacid forms the proton-transfer contact pair, which accumulates and splits into reaction products by proton diffusion on a longer timescale. In contrast, both proton dissociation and contact-pair splitting stages proceed at significantly lower rates in HNBI. The latter implies that the contact pair is trapped by small energy barriers hindering recombination (k_{-1}) and splitting (k_2). The model departs here slightly from the classical Eigen–Weller mechanism, which assumes that the splitting of the pair is controlled by diffusion. In turn, we find indication of a non-negligible hydrogen-bond interaction in the proton-transfer pair of a moderately strong acid. This interaction slows down splitting and formation of the pair. This work provides a complete set of microscopic rate constants for the elementary proton transfer to solvent reaction in alcohols, which are essential to benchmark reaction models. Furthermore, it defines the conditions under which the proton-transfer contact pair predominates and thus opens the door to the spectroscopic characterization of an elusive reaction intermediate.

Experimental Section

HNBI was prepared as described in Reference 25. Steady-state UV–vis absorption spectra were scanned in a Cary 3E spectrophotometer (Varian). Fluorescence spectra were acquired in a Spex Fluoromax-2 fluorometer and were corrected for instrumental factors. Fluorescence decay curves were measured by the time-correlated single photon counting technique in an Edinburgh Instruments LifeSpec-ps time-resolved spectrofluorometer. Excitation was performed at magic angle polarization with 60 ps pulses centered at 371 nm (Picoquant). Fitting routines were programmed with MATLAB R2012a. See Supporting Information for further details.

Acknowledgement

We thank the Spanish Government and the European Regional Development Fund (Grants CTQ2010-17835 and CTQ2010-17026) and the Xunta de Galicia (Grants CN 2012/314, EM2012/091 and GPC2013/052) for financial support of our work. JLPL thanks the Spanish Ministry of Economy and Competitiveness for funding through the *Ramón y Cajal* Programm 2009. MV and AB thank the Spanish Government and the "Segundo Gil-Dávila" Foundation, respectively, for financial support. We thank Sergey A. Kovalenko for a critical reading of the manuscript.

Supporting Information Available

Detailed experimental section, comparison of biexponential and triexponential global fits, and thorough description of global and target analysis.

This material is available free of charge via the Internet at `http://pubs.acs.org/`.

References

(1) Eigen, M. Proton Transfer, Acid-Base Catalysis, and Enzymatic Hydrolysis. Part I. Elementary Processes. *Angew. Chem. Int. Edit.* **1964**, *3*, 1–19.

(2) Bell, R. P. *The Proton in Chemistry*; Chapman and Hall: London, U. K., 1973.

(3) Agmon, N. Elementary Steps in Excited-State Proton Transfer. *J. Phys. Chem. A* **2005**, *109*, 13–35.

(4) Ädelroth, P. Special Issue on Proton Transfer in Biological Systems. *Biochim. Biophys. Acta (BBA) - Bioenergetics* **2006**, *1757*, 867–870.

(5) Silverman, L. N.; Spry, D. B.; Boxer, S. G.; Fayer, M. D. Charge Transfer in Photoacids Observed by Stark Spectroscopy. *J. Phys. Chem. A* **2008**, *112*, 10244–10249.

(6) Spry, D. B.; Fayer, M. D. Charge Redistribution and Photoacidity: Neutral versus Cationic Photoacids. *J. Chem. Phys.* **2008**, *128*, 084508.

(7) Warshel, A. Dynamics of Reactions In Polar-solvents - Semi-classical Trajectory Studies of Electron-transfer and Proton-transfer Reactions. *J. Phys. Chem.* **1982**, *86*, 2218–2224.

(8) Ando, K.; Hynes, J. T. Molecular Mechanism of HCl Acid Ionization in Water: Ab Initio Potential Energy Surfaces and Monte Carlo Simulations. *J. Phys. Chem. B* **1997**, *101*, 10464–10478.

(9) Kiefer, P. M.; Hynes, J. T. Adiabatic and Nonadiabatic Proton Transfer Rate Constants in Solution. *Solid State Ionics* **2004**, *168*, 219–224.

(10) Kiefer, P. M.; Hynes, J. T. Theoretical Aspects of Tunneling Proton Transfer Reactions in a Polar Environment. *J. Phys. Org. Chem.* **2010**, *23*, 632–646.

(11) Soudackov, A. V.; Hazra, A.; Hammes-Schiffer, S. Multidimensional Treatment of Stochastic Solvent Dynamics in Photoinduced Proton-Coupled Electron Transfer Processes: Sequential, Concerted, and Complex Branching Mechanisms. *J. Chem. Phys.* **2011**, *135*, 144115.

(12) Hammes-Schiffer, S. When Electrons and Protons Get Excited. *Proc. Natl. Acad. Sci. U.S.A.* **2011**, *108*, 8531–8532.

(13) Maurer, P.; Thomas, V.; Iftimie, R. A Computational Study of Ultrafast Acid Dissociation and Acid-Base Neutralization Reactions. II. The Relationship Between the Coordination State of Solvent Molecules and Concerted versus Sequential Acid Dissociation. *J. Chem. Phys.* **2011**, *134*, 094505.

(14) Beens, H.; Grellmann, K. H.; Gurr, M.; Weller, A. H. Effect of Solvent and Temperature on Proton Transfer Reactions of Excited Molecules. *Discuss. Faraday Soc.* **1965**, *39*, 183–193.

(15) Tolbert, L.; Solntsev, K. Excited-State Proton Transfer: From Constrained Systems to "Super" Photoacids to Superfast Proton Transfer. *Acc. Chem. Res.* **2002**, *35*, 19–27.

(16) Perez-Lustres, J. L.; Rodriguez-Prieto, F.; Mosquera, M.; Senyushkina, T. A.; Ernsting, N. P.; Kovalenko, S. A. Ultrafast Proton Transfer to Solvent: Molecularity and Intermediates from Solvation- and Diffusion-Controlled Regimes. *J. Am. Chem. Soc.* **2007**, *129*, 5408–5418.

(17) Spry, D. B.; Goun, A.; Fayer, M. D. Deprotonation Dynamics and Stokes Shift of Pyranine (HPTS). *J. Phys. Chem. A* **2007**, *111*, 230–237.

(18) Veiga Gutierrez, M.; Brenlla, A.; Carreira Blanco, C.; Fernandez, B.; Kovalenko, S. A.; Rodriguez-Prieto, F.; Mosquera, M.; Perez Lustres, J. L. Dissociation of a Strong Acid in Neat Solvents: Diffusion is Observed After Reversible Proton Ejection Inside the Solvent Shell. *J. Phys. Chem. B* **2013**, *117*, 14065–14078.

(19) Thomas, V.; P., M.; Iftimie, R. On the Formation of Proton-Shared and Contact Ion Pair Forms during the Dissociation of Moderately Strong Acids: An Ab Initio Molecular Dynamics Investigation. *J. Phys. Chem. B* **2010**, *114*, 8147–8155.

(20) Wang, S.; Bianco, R.; Hynes, J. T. An Atmospherically Relevant Acid: HNO_3. *Comput. Theor. Chem.* **2011**, *965*, 340–345.

(21) Sano, H.; Tachiya, M. Partially Diffusion-Controlled Recombination. *J. Chem. Phys.* **1979**, *71*, 1276–1282.

(22) Pines, E.; Huppert, D. Geminate Recombination Proton-transfer Reactions. *Chem. Phys. Lett.* **1986**, *126*, 88–91.

(23) Gould, E.-A.; Popov, A. V.; Tolbert, L. M.; Presiado, I.; Erez, Y.; Huppert, D.; Solntsev, K. M. Excited-State Proton Transfer in N-Methyl-6-Hydroxyquinolinium Salts: Solvent and Temperature Effects. *Phys. Chem. Chem. Phys.* **2012**, *14*, 8964–8973.

(24) Lustres, J. L. P.; Kovalenko, S. A.; Mosquera, M.; Senyushkina, T.; Flasche, W.; Ernsting, N. P. Ultrafast Solvation of N-Methyl-6-Quinolone Probes Local IR Spectrum. *Angew. Chem., Int. Ed.* **2005**, *44*, 5635–5639.

(25) Brenlla, A.; Rodriguez-Prieto, F.; Mosquera, M.; Rios, M. A.; Rios Rodriguez, M. C. Solvent-Modulated Ground-State Rotamerism and Tautomerism and Excited-State Proton-Transfer Processes in o-Hydroxynaphthylbenzimidazoles. *J. Phys. Chem. A* **2009**, *113*, 56–67.

(26) Löfroth, J.-E. Time-Resolved Emission Spectra, Decay-Associated Spectra, and Species-Associated Spectra. *J. Phys. Chem.* **1986**, *90*, 1160–1168.

(27) Kiefer, P. M.; Hynes, J. T. Kinetic Isotope Effects for Adiabatic Proton Transfer Reactions in a Polar Environment. *J. Phys. Chem. A* **2003**, *107*, 9022–9039.

SUPPORTING INFORMATION OF "A Moderately Strong Photoacid Dissociates in Alcohols with High Transient Concentration of the Proton-Transfer Contact Pair"

Alfonso Brenlla,[†,‡] Manoel Veiga Gutiérrez,[†,¶] M. Carmen Ríos Rodríguez,[†] Flor Rodríguez-Prieto,[†] Manuel Mosquera,[*,†] and J. Luis Pérez Lustres[*,†]

Center for Research in Biological Chemistry and Molecular Materials (CIQUS) and Department of Physical Chemistry, University of Santiago de Compostela, E-15782 Santiago de Compostela (Spain)

E-mail: manuel.mosquera@usc.es; luis.lustres@usc.es

Phone: +34 8818 15722. Fax: +34 8818 15704

[*]To whom correspondence should be addressed
[†]CIQUS
[‡]now at Department of Chemistry, Wayne State University, 5101 Cass Avenue, Detroit, MI 48202 (USA)
[¶]now at PicoQuant GmbH, Kekuléstr. 7, 12489 Berlin (Germany)

Sample preparation and materials

2-(1'-hydroxy-2'-naphtyl)benzimidazole (HNBI) was prepared as described previously.[1] Solutions were freshly prepared in spectroscopic grade non-degassed solvents from Aldrich and Scharlau. The acidity was set by adding corresponding amounts of $HClO_4$ (70% Fluka). Typically, sample concentration was of the order of 10^{-4} M for steady-state absorption measurements and around 10^{-5} M for fluorescence.

Absorption and fluorescence spectroscopy

Steady-state UV–vis absorption spectra were scanned in a Varian Cary 3E double-beam spectrophotometer. Fluorescence spectra were acquired in an Spex Fluoromax 2 fluorometer at right angle geometry. Fluorescence spectra were corrected for instrumental factors by multiplying by correction functions supplied by the manufacturer.

Fluorescence decay curves were measured by the time-correlated single photon counting technique (TC-SPC) in an Edinburgh Instruments LifeSpec-ps time-resolved spectrofluorometer. The system is equipped with a diode laser as excitation source (Picoquant LDH-P-C-375 controlled by a PDL 800-B unit, $\lambda_{max} = 371$ nm, maximum repetition rate 40 MHz, 60 ps FWHM and $10 - 30$ pJ/pulse). A microchannel plate photomultiplier (Hamamatsu R3809U-50) with 50 ps response time and detection range of $200 - 850$ nm was used as detector. The repetition rate of the excitation source was set to 2.5 MHz and 5000 counts were acquired in the maximum at counting rates of less than 125 kHz. The multichannel analyzer has 4096 channels with minimum width of 0.61 ps/channel. Magic angle polarization was employed. The instrument response function was obtained by monitoring the scattered light at the most intense Raman band of the corresponding solvent.

All steady-state absorption and fluorescence measurements were done in 1 cm-thick fused-silica cuvettes and slit widths were chosen so that acceptable signal-to-noise ratios were reached: 2 nm of absorption, 8 nm for fluorescence and 16 nm for TC-SPC.

Floats

Biexponential versus Triexponential Global Fits

This subsection is devoted to demonstrate the adequacy of the triexponential global fit. Figure SI 1 shows the same data set as in Figure 2 of the manuscript together with a biexponential global fit. Compared with the triexponential fit in Figure 2, the χ^2_N values are slightly larger and the residuals are less homogeneously distributed around null. However, the differences between the two kinds of fits are non conclusive. This can be anticipated in view of the similar values of τ_1 and τ_2 in methanol. However, the difference becomes obvious in solvents where both decay times are more dissimilar. Figures SI 2 and 3 show the results of the global biexponential and triexponential fits in ethanol, respectively, whereas Figures SI 4 and 5 show the same information for deuterated ethanol. The triexponential fits are clearly better than the biexponential ones in those solvents. The same is observed for 1-propanol. It seems reasonable to conclude that the same kinetics holds for methanol but the similarity of the lifetimes hinders a more clear observation.

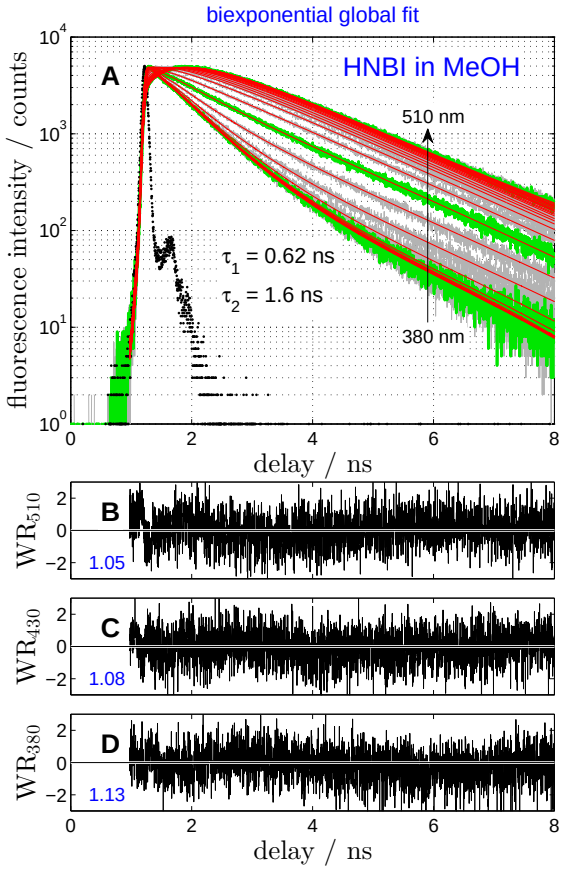

Figure SI 1: Fluorescence decay curves of HNBI measured from 380 to 510 nm every 5 nm in methanol (gray lines, Panel A). Results from a global **biexponential** fit (red lines) are shown together with the excitation pulse (black dots). Green curves highlight three representative wavelengths for which weighted residuals (WR_λ) are shown in panels B-D, where normalized χ^2_N values are indicated in blue for each emission wavelength.

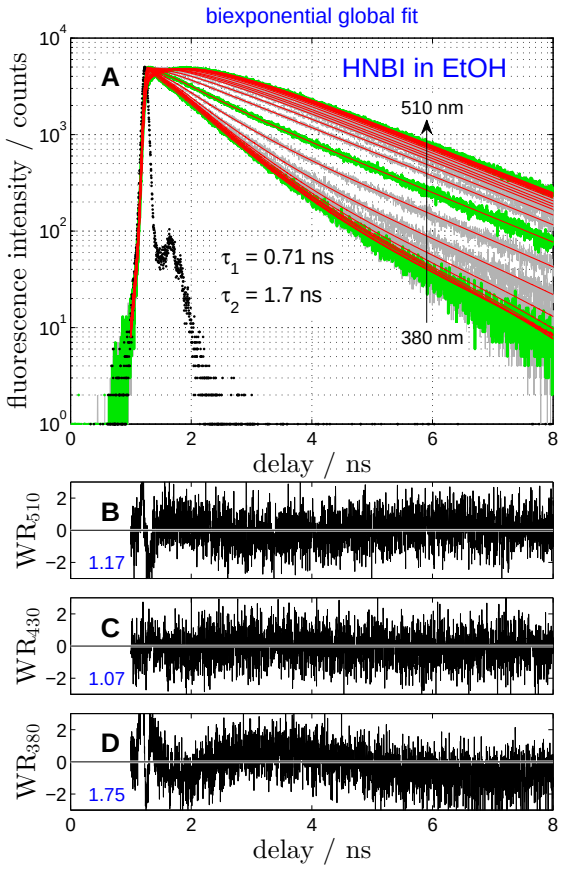

Figure SI 2: Fluorescence decay curves of HNBI measured from 380 to 510 nm every 5 nm in ethanol (gray lines, Panel A). Results from a global **biexponential** fit (red lines) are shown together with the excitation pulse (black dots). Green curves highlight three representative wavelengths for which weighted residuals (WR_λ) are shown in panels B-D, where normalized χ^2_N values are indicated in blue for each emission wavelength.

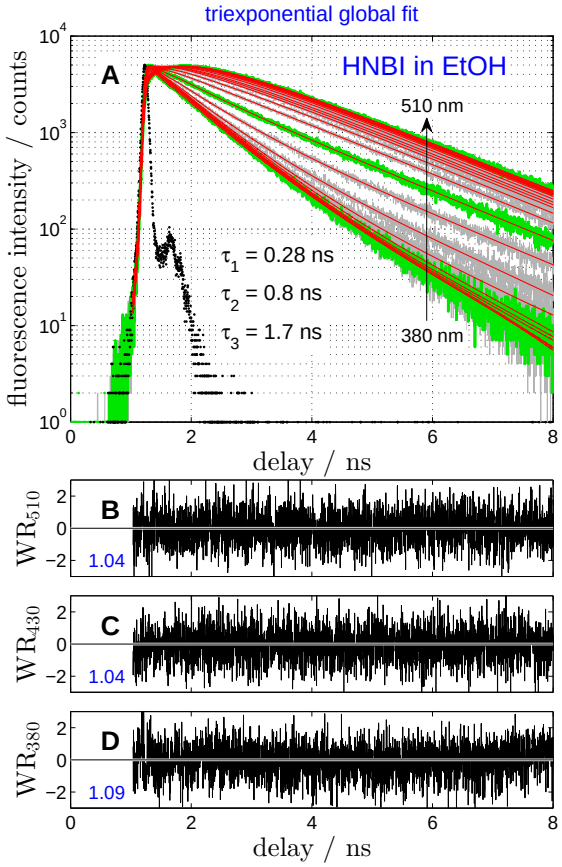

Figure SI 3: Fluorescence decay curves of HNBI measured from 380 to 510 nm every 5 nm in ethanol (gray lines, Panel A). Results from a global **triexponential** fit (red lines) are shown together with the excitation pulse (black dots). Green curves highlight three representative wavelengths for which weighted residuals (WR_λ) are shown in panels B-D, where normalized χ^2_N values are indicated in blue for each emission wavelength.

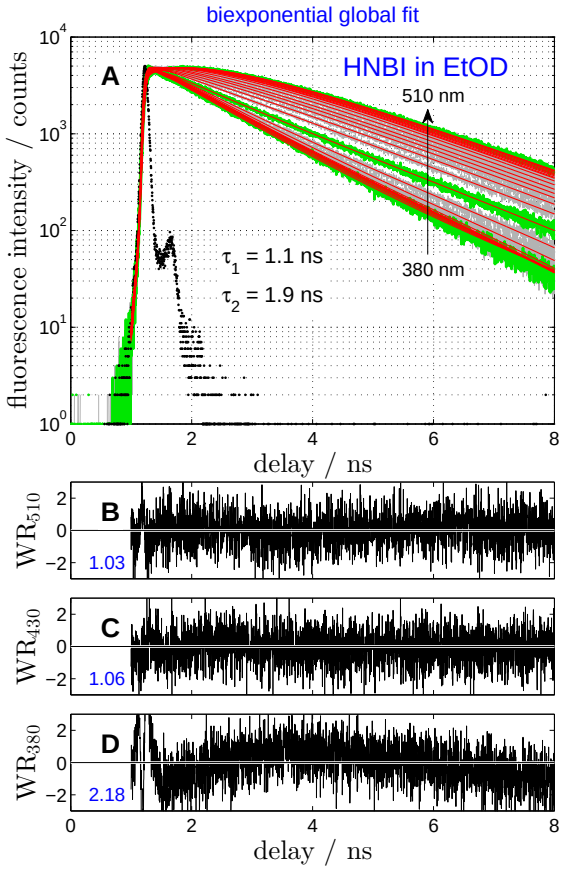

Figure SI 4: Fluorescence decay curves of HNBI measured from 380 to 510 nm every 5 nm in deuterated ethanol (gray lines, Panel A). Results from a global **biexponential** fit (red lines) are shown together with the excitation pulse (black dots). Green curves highlight three representative wavelengths for which weighted residuals (WR_λ) are shown in panels B-D, where normalized χ^2_N values are indicated in blue for each emission wavelength.

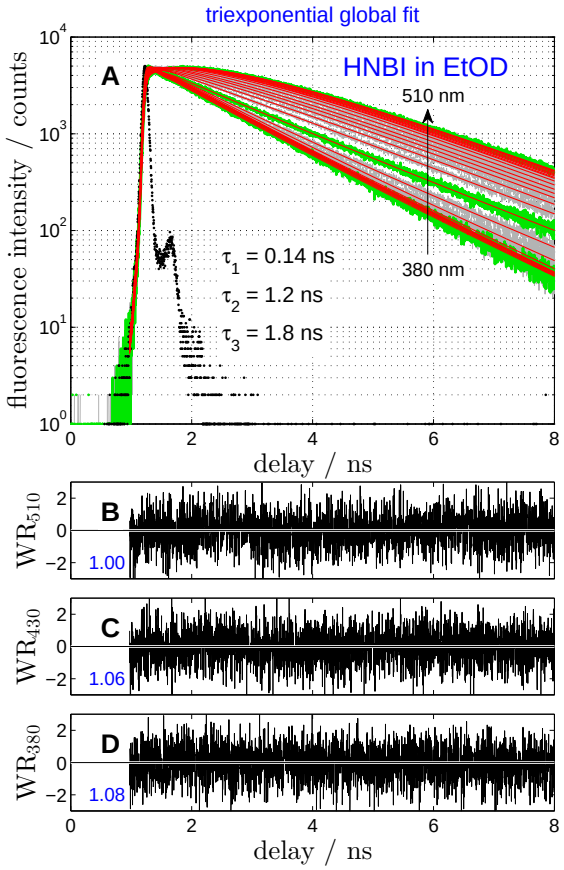

Figure SI 5: Fluorescence decay curves of HNBI measured from 380 to 510 nm every 5 nm in deuterated ethanol (gray lines, Panel A). Results from a global **triexponential** fit (red lines) are shown together with the excitation pulse (black dots). Green curves highlight three representative wavelengths for which weighted residuals (WR_λ) are shown in panels B-D, where normalized χ^2_N values are indicated in blue for each emission wavelength.

Global Triexponential Fit of Fluorescence Decay Traces

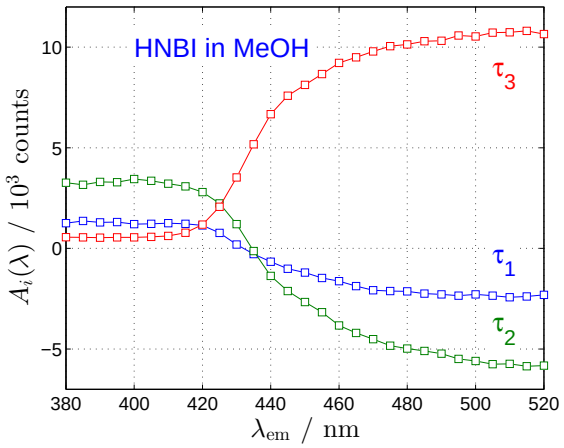

Figure SI 6: Time-zero amplitudes associated to the exponential terms $\exp(-t/\tau_1)$ (blue), $\exp(-t/\tau_2)$ (green) and $\exp(-t/\tau_3)$ (red) as function of the emission wavelength scanned for the photodissociation of HNBI in methanol. Values obtained by a global triexponential fit performed over 29 emission wavelengths.

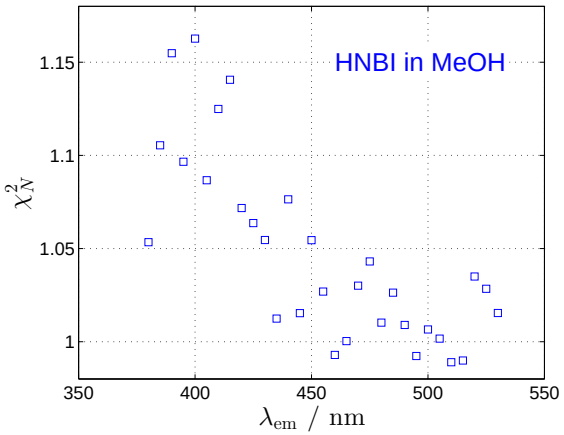

Figure SI 7: Local χ^2_N values obtained in the global triexponential fit of the fluorescence decay curves measured for the photodissociation of HNBI in methanol.

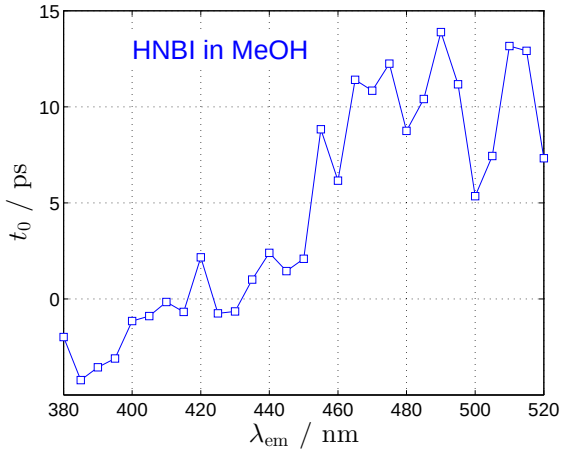

Figure SI 8: t_0 delay times obtained in the global triexponential fit of the fluorescence decay curves measured for the photodissociation of HNBI in methanol.

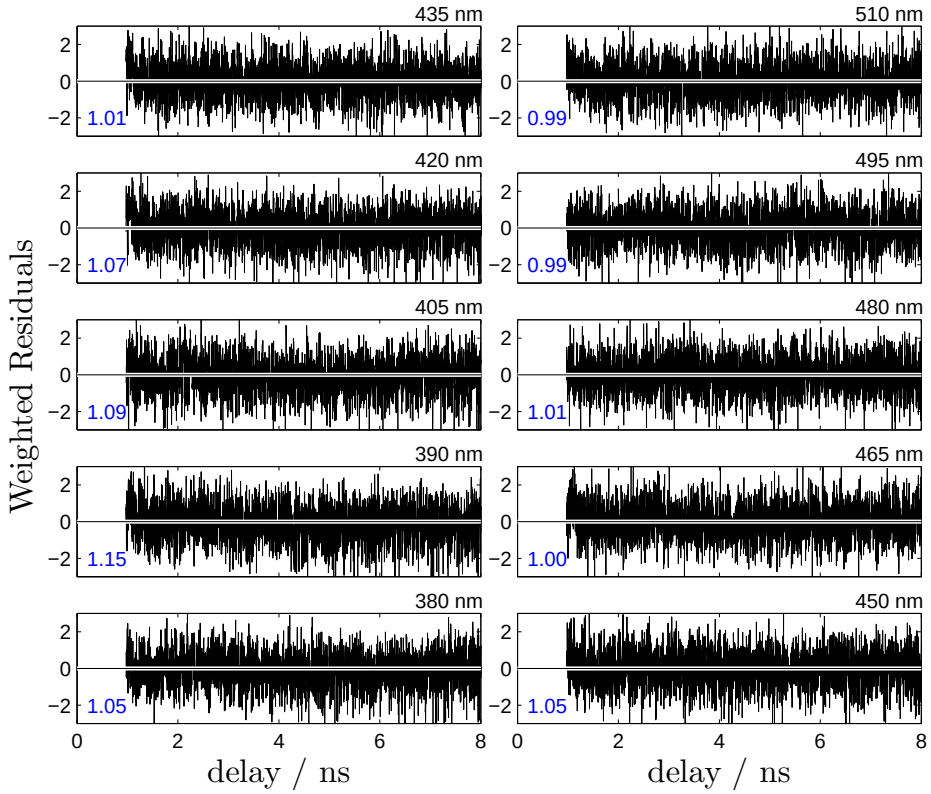

Figure SI 9: Weighted residuals obtained in the global triexponential fit of the fluorescence decay curves measured for the photodissociation of HNBI in methanol. Emission wavelengths and local χ^2_N values are indicated for each data set.

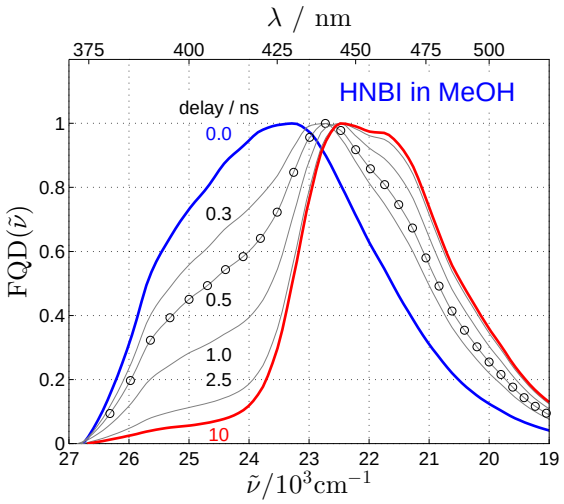

Figure SI 10: Reconstructed time-resolved fluorescence emission spectra of HNBI in methanol, shown as fluorescence quantum distribution over wavenumbers. The black empty circles indicate the individual wavelengths at which fluorescence decay measurements were performed. The lines correspond to cubic Hermite interpolations to the experimental data. The time delays are indicated in nanoseconds by legends close to each curve.

Target Analysis (Global Fit Assuming the Kinetic Model in Scheme 2)

Table SI 1: Rate constants (in ns^{-1}) obtained from the target analysis of fluorescence decay curves.

Solvent	$[HClO_4]$/M	β_1	β_2	β_3	X
methanol	0.01	2.31 ± 0.13	1.35 ± 0.05	0.647 ± 0.002	1.68 ± 0.01
ethanol	0.01	2.68 ± 0.08	1.14 ± 0.02	0.585 ± 0.001	1.56 ± 0.01
ethanol-d	0.01	1.74 ± 0.06	0.75 ± 0.01	0.563 ± 0.001	0.88 ± 0.01
ethanol	0.10	3.07 ± 0.10	1.29 ± 0.02	0.575 ± 0.001	1.79 ± 0.01
propanol	0.01	3.10 ± 0.06	0.81 ± 0.01	0.553 ± 0.001	1.19 ± 0.01

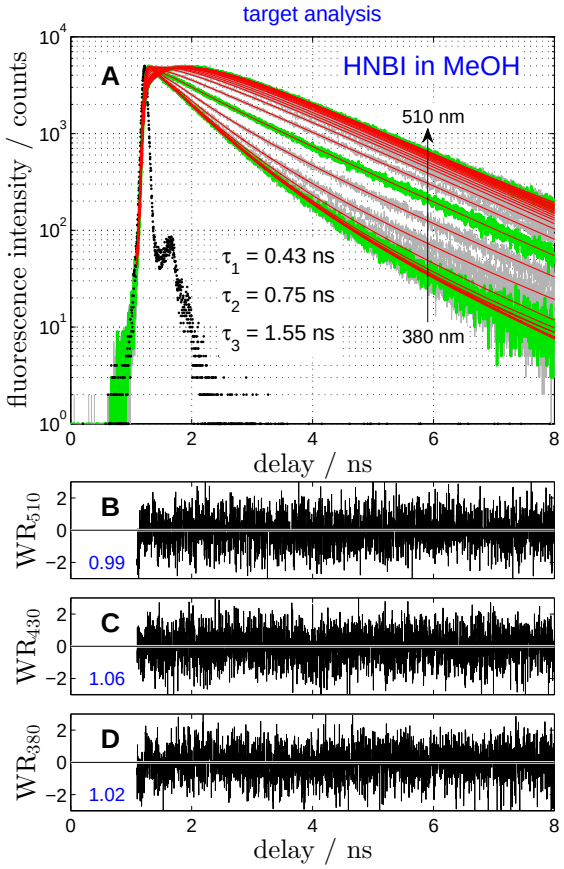

Figure SI 11: Panel A: fluorescence decay curves measured for the photodissociation of HNBI in methanol (gray lines). The red lines show the global fits performed with the concentration profiles derived from the model in Scheme 2 (target analysis). The resulting decay times are shown as inset. The excitation pulse is also shown (black dots). The green curves mark three representative wavelengths for which residuals (WR_λ) are shown in panels B-D for the emission wavelengths λ. The latter contain local χ^2_N values in blue.

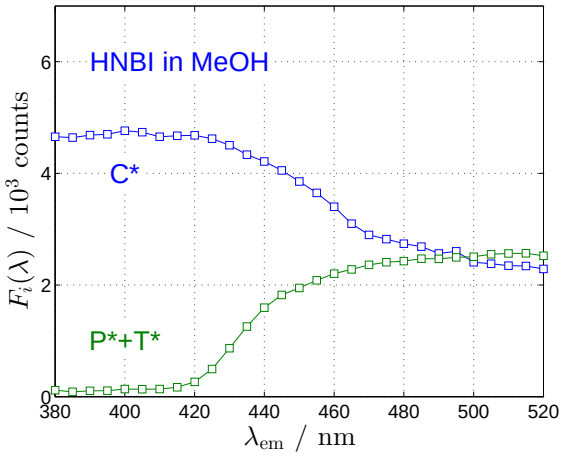

Figure SI 12: Pre-factors multiplying the concentrations of **C*** (blue squares) and (**P***+**T***) (green squares) as obtained from the target analysis of the fluorescence decay curves measured for the photodissociation of HNBI in methanol.

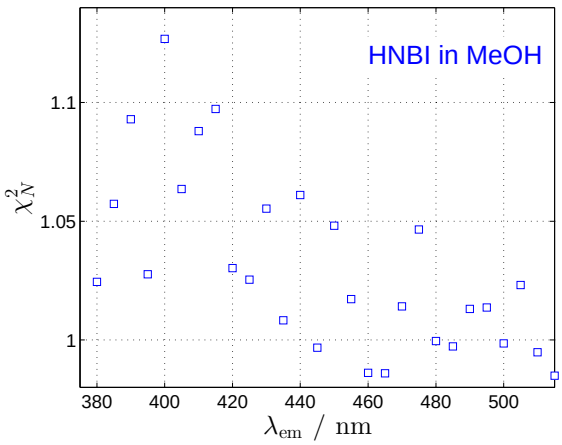

Figure SI 13: Local χ^2_N values obtained in the global fit of the fluorescence decay curves measured for the photodissociation of HNBI in methanol when the concentrations of the emitting species are assumed to follow the analytical forms in Equations (1) (target analysis).

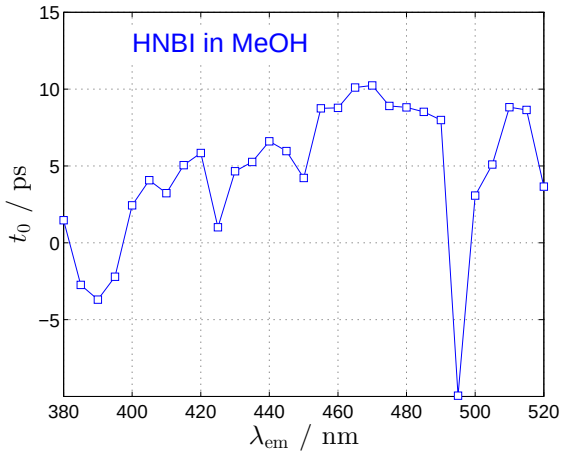

Figure SI 14: t_0 delay times obtained in the global fit of the fluorescence decay curves measured for the photodissociation of HNBI in methanol when the concentrations of the emitting species are assumed to follow the analytical forms in Equations (1) (target analysis).

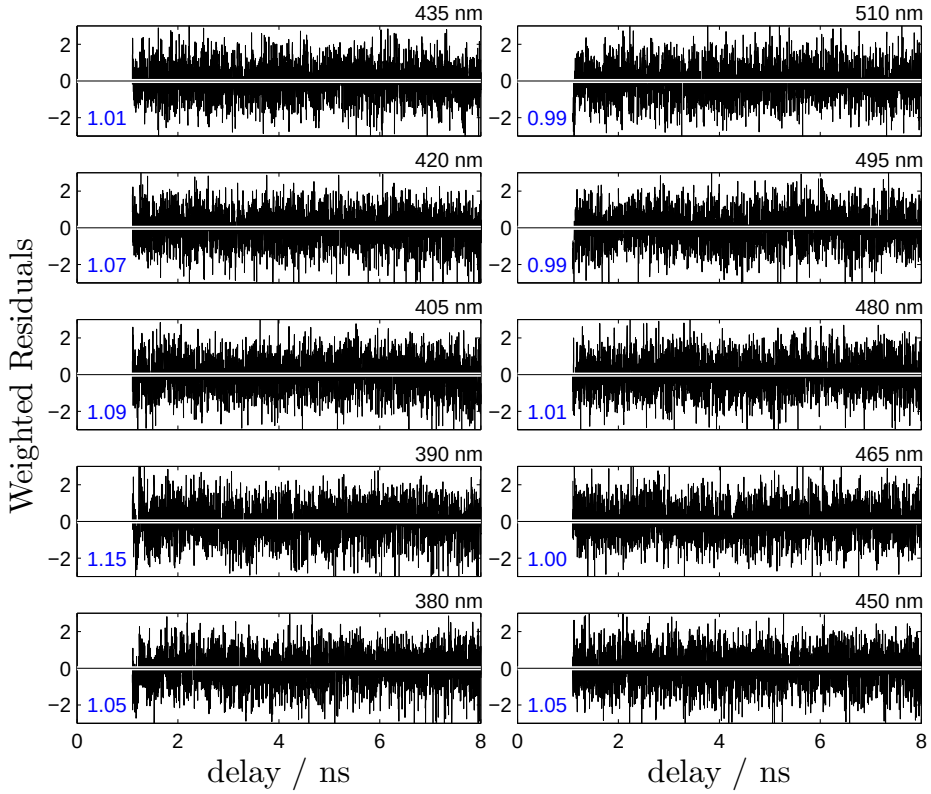

Figure SI 15: Weighted residuals obtained in the global fit of the fluorescence decay curves measured for the photodissociation of HNBI in methanol when the concentrations of the emitting species are assumed to follow the analytical forms in Equations (1) (target analysis). Emission wavelengths and local χ^2_N values are indicated for each data set.

References

(1) Brenlla, A.; Rodriguez-Prieto, F.; Mosquera, M.; Rios, M. A.; Rios Rodriguez, M. C. Solvent-Modulated Ground-State Rotamerism and Tautomerism and Excited-State Proton-Transfer Processes in o-Hydroxynaphthylbenzimidazoles. *J. Phys. Chem. A* **2009**, *113*, 56–67.